

CrossMark
click for updatesCite this: *RSC Adv.*, 2017, 7, 6538

SO₂ capture by ionic liquid and spectroscopic speciation of sulfur(IV) therein†

Y. Yasaka,* K. Watanabe and Y. Kimura*

The absorption of equimolar sulfur dioxide (SO₂) by tributyl-octylphosphonium bicarbonate ([P₄₄₄₈][HCO₃]) resulted in the formation of a corresponding bisulfite ionic liquid ([P₄₄₄₈][bisulfite]) accompanied by carbon dioxide (CO₂) release. The liquid formed absorbed an additional 0.6 equivalents of SO₂. The speciation of sulfur(IV) in the SO₂-loaded ionic liquid was performed using Raman and NMR spectroscopies. The two known isomeric forms of bisulfite ion in aqueous systems were identified while the condensation of bisulfite anion was suppressed in [P₄₄₄₈][bisulfite]. The isomer with the proton bonded to the sulfur atom (HSO₃[−]) was more abundant than the one with the proton bonded to the oxygen atom (HOSO₂[−]). The isomeric exchange rate was much slower in the IL than in water as distinguished by ¹H NMR. When excess SO₂ was absorbed by [P₄₄₄₈][bisulfite], the presence of molecular SO₂ and HS₂O₅[−] were suggested by Raman bands as an indication of concerted physisorption and chemisorption.

Received 20th October 2016
Accepted 10th January 2017

DOI: 10.1039/c6ra25528k

www.rsc.org/advances

Introduction

Sulfur dioxide is an environmental pollutant emitted in large amounts wherever petroleum is burnt. The onsite capture of sulfur dioxide by a liquid absorbent is an option to address the pollution issue. Ionic liquids (ILs) are liquid salts that are derived from organic cations. They are practically nonvolatile and can capture various gases.¹ Although there are numerous studies on the carbon dioxide (CO₂) capture by ILs,^{1–19} the studies on the SO₂ capture by ILs are rather limited. The physisorption of SO₂ by ILs has been demonstrated by J. L. Anderson *et al.*²⁰ for 1-*n*-hexyl-3-methylimidazolium bis(trifluoromethylsulfonyl)imide and 1-*n*-hexyl-3-methylpyridinium bis(trifluoromethylsulfonyl)imides. These two ILs absorb nearly equimolar SO₂ at 25 °C and 0.1 MPa. Interestingly, the absorption capacity of SO₂ and CO₂ as a function of pressure can be roughly scaled by the reduced pressure, which is the actual pressure divided by the saturation pressure of each gas at the measurement temperature.²⁰ In attempt to attain even

higher absorption capacity (especially in weight basis) and/or in targeting absorptions at lower SO₂ pressures, a number of “functionalized ILs” have been developed.^{21–29} It has been found that several functional groups are in particular effective for enhancing SO₂ absorption. These include X[−] (X = halogen),²¹ −NH₂ (amino),^{22,23} −O[−] (alkoxide and phenoxide),²⁴ −COO[−] (carboxylate),^{25–28} −SO₃[−] (sulfonate),²⁶ −N[−]−CO− (acylamide)²⁹ groups, all of which have electron-rich atoms. Actual chemical forms of sulfur in these absorbents are not well understood. Based on the vibrational spectral shift of SO₂ and the colour change of the solution by absorption, it is argued that charge-transfer interaction is operating when SO₂ is absorbed by 1-butyl-3-methylimidazolium bromide.²¹

SO₂ is an acid oxide and thus can be captured by bases, as is done in wet limestone scrubbing process. The usage of ILs with basic anion component is especially attractive for capturing SO₂. In the present study we demonstrate SO₂ absorption by a newly synthesized IL, tributyl-octylphosphonium bicarbonate ([P₄₄₄₈][HCO₃]). From spectroscopic analysis we show that this IL absorbs an equimolar of SO₂ via “gas exchange” reaction (eqn (1)).



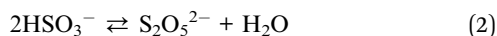
Interestingly we also find that the IL can capture additional SO₂, after completion of eqn (1). It is quite an interesting issue how SO₂ molecules are dissolved in the IL.

It has been known that bisulfite ion is subject to complicated equilibria in aqueous solutions.^{30–32} Raman spectroscopy has provided evidence of condensation (eqn (2)) and isomerization (eqn (3)) equilibria for bisulfite ions.^{30–39}

Department of Molecular Chemistry and Biochemistry, Faculty of Science and Engineering, Doshisha University, Kyotanabe, Kyoto 610-0321, Japan. E-mail: yokimura@mail.doshisha.ac.jp

† Electronic supplementary information (ESI) available: Tables of thermal energies, geometries of the optimized structures of monomers and clusters by DFT calculations, table of experimentally observed Raman shifts, tables of calculated Raman shift and assignments of anions, ¹H NMR, ¹³C NMR, IR, and HR-MS spectra of [P₄₄₄₈][HCO₃], ¹³C NMR of SO₂ loaded [P₄₄₄₈][HCO₃], figures of images for the optimized structures of monomers and clusters by DFT calculations, explanations of the multi-peak fitting, figures of calculated Raman activities of anions in SCRF water, and of dimers of HOSO₂[−], and of complexes of bisulfite with SO₂, temperature dependence of the ¹H NMR. See DOI: 10.1039/c6ra25528k





The hydrogen atom is directly bonded with the sulfur atom in the left-hand side of eqn (3), while the hydrogen atom is bonded with the oxygen atom in the right hand side of eqn (3). Note that the isomer on the right in eqn (3) is present only in solution and its identity is not fully determined. The assignment of sulfur Raman bands in water have been debated for several decades. The coexistence of many structurally different but somewhat similar chemical species often induced confusions about overlapped and closely placed bands. The HSO_3^- isomer is identified by combined Raman/X-ray³³ and Raman/neutron³⁴ analysis of solid CsDSO_3 . It is characterized in aqueous solution as well by vibrational spectroscopy owing to the well resolved band of the SH stretching mode at 2530 cm^{-1} (ν_{SH}). The disulfite ion can be also isolated as a crystalline compound⁴⁰ and strong Raman bands have been unambiguously assigned.³⁵ For other species, they are metastable and are always accompanied by equilibrium “contaminants”. The presence of HOSO_2^- isomer in aqueous solution has been deduced from Raman spectroscopic observation³⁶ and later supported by NMR,⁴¹ XANES,³⁴ and computational studies.^{42–44} There are also several speculative discussions on the existence of the dimers of sulfite anion,^{37,45} and several bands remain unassigned. In the present study, analysis of the sulfite Raman bands in the IL is carried out, which in turn aids in confirming the band assignments in aqueous systems.

NMR spectroscopy is complementary to Raman spectroscopy, particularly for quantification. A series of ^{17}O NMR spectroscopic studies have been carried out by Horner *et al.* to investigate the equilibrium constants and the rates of eqn (2) and (3) in aqueous solutions.^{41,46} Although ^{17}O NMR spectroscopy is straightforward for sulfur(IV) oxoanions, it gives limited information regarding the IL due to severe line broadening. Alternatively, ^1H NMR provides direct evidence for the bisulfite isomerization in eqn (3) owing to the slowdown of the chemical exchange. In this work, we performed combined NMR and Raman spectroscopic investigations on the sulfur(IV) speciation in ILs to shed light on the absorption mechanism of SO_2 by ILs.

Experimental

Sample preparation

The IL, tributyl(octyl)phosphonium bicarbonate ($[\text{P}_{4448}]\text{HCO}_3$) was obtained as follows. Bromooctane (Wako Chemicals) was reacted with 0.9 equiv. of tributylphosphine (Wako Chemicals) at $108\text{ }^\circ\text{C}$ for 24 h. The obtained liquid (crude $[\text{P}_{4448}]\text{Br}$) was shaken vigorously with 1.1 equiv. of aqueous KPF_6 (Aldrich) and dichloromethane. The separation of two phases yielded dichloromethane solution of $[\text{P}_{4448}]\text{PF}_6$. Upon evaporation of dichloromethane, the crude $[\text{P}_{4448}]\text{PF}_6$ was recrystallized 3 times from methanol at $-40\text{ }^\circ\text{C}$. The purified and dried $[\text{P}_{4448}]\text{PF}_6$ showed its melting point of $36\text{ }^\circ\text{C}$. The 2-propanol solution of $[\text{P}_{4448}]\text{PF}_6$ was mixed with 1.1 equiv. of 2-propanol solution of CsOH (Nacalai Tesque) and hexane (30 wt%). The precipitates

(CsPF_6) were filtered twice at $-80\text{ }^\circ\text{C}$. To the filtrate, excess CO_2 was bubbled in and the resultant solution was stirred with active carbon overnight. After filtration, the filtrate was evacuated at $30\text{ }^\circ\text{C}$ for solvent removal. The residue was diluted with benzene, and then filtered and evacuated to yield $[\text{P}_{4448}]\text{HCO}_3$ as highly viscous and almost colourless liquid. The compound was characterized by NMR, IR, and HR-MS which are given at the footnote[‡] and in Fig. S1 of the ESI.[†]

The SO_2 gas was prepared by the action of concentrated sulfuric acid (Nacalai Tesque) to $\text{Na}_2\text{S}_2\text{O}_5$ (Nacalai Tesque). The evolved SO_2 was transferred to a syringe (100 mL) and then injected into an evacuated 300 mL flask containing 10 g of $[\text{P}_{4448}]\text{HCO}_3$. The IL was stirred for 30 min to ensure uptake of SO_2 . Then approximately 0.7 g of the liquid was withdrawn to an NMR tube for NMR and Raman spectroscopic measurements. To the rest of the liquid, additional injections of SO_2 were performed in a similar manner to obtain samples at higher SO_2 loadings.

In the present work, SO_2 loadings in the IL is reported by the mole ratio q_{SO_2} , which is defined by the mole of SO_2 absorbed by the liquid divided by the mole of the $[\text{P}_{4448}]$ cation. Specifically, $q_{\text{SO}_2} = 1$ corresponds to “pure” $[\text{P}_{4448}][\text{bisulfite}]$. We use the notation $[\text{bisulfite}]$ for including all plausible isomers of HSO_3^- . The ^1H and ^{13}C NMR data for $[\text{P}_{4448}][\text{bisulfite}]$ are given at the footnote.[§] The q_{SO_2} of each sample was calculated by the volume of SO_2 injected to the reactor vessel. Nevertheless, this may overestimate the actual loading when part of SO_2 injected remained in the gas phase of the reactor at equilibrium. Thus we checked the q_{SO_2} directly by wet titration method for selected samples as follows. After the spectroscopic measurements were finished, the sample was dissolved in water and immediately oxidized by the action of excess KMnO_4 . The excess KMnO_4 was reduced by oxalic acid until the purple colour disappears. To the solution, ammonia solution was added to precipitate Mn^{2+} from the solution. The moles of SO_4^{2-} (which is equal to the loading of SO_2) was determined by the standard back titration method using aqueous BaCl_2 and disodium salts of EDTA as titrants and phthalein complex as an indicator. On the other hand, the mole of the $[\text{P}_{4448}]$ cation was determined by the integral of ^{31}P NMR peak (34 ppm) within an accuracy of 2%. Thus obtained values of q_{SO_2} was consistent ($\pm 10\%$) with that determined by the injected volume, indicating that injected SO_2 was quantitatively absorbed by the IL up to $q_{\text{SO}_2} \sim 1.6$ at atmospheric pressure.

NMR measurements

NMR spectra were obtained using a JEOL ECA300 (8.4 T) magnet equipped with a standard 5 mm probe (TH5AT). The ^1H NMR spectra were scanned > 8 times with a repetition time of 60 s.

[‡] $[\text{P}_{4448}]\text{HCO}_3$: ^1H NMR: δ 0.8 (br), 1.2–1.6(br), 2.6(br), (δ 0.8–2.6 44H), 11.3(br, $1.01 \pm 0.03\text{H}$). ^1H NMR (H_2O with 0.20% w/w STSP): δ 0.85–0.93 (m, 12H), 1.23–1.33 (m, 8H), 1.40–1.60 (m, 16H), 2.13 (m, 8H). $^{13}\text{C}\{^1\text{H}\}$ NMR (H_2O): δ 12.88 (3C), 13.85 (1C), 17.95 (d, $J_{\text{CP}} = 190\text{ Hz}$, 4C), 20.88 (d, $J_{\text{CP}} = 18\text{ Hz}$, 1C), 22.41 (1C), 23.00 (d, $J_{\text{CP}} = 18\text{ Hz}$, 3C), 23.51 (d, $J_{\text{CP}} = 60\text{ Hz}$, 3C), 28.25 (1C), 18.47 (1C), 30.06 (d, $J_{\text{CP}} = 60\text{ Hz}$, 1C), 31.47 (1C), 160.49 (1C).

[§] $[\text{P}_{4448}][\text{bisulfite}]$ (no solvent): δ 0.8(br), 1.2–1.6(br), 2.6(br) (δ 0.8–2.6 44H), 4.06(s, 0.47H), 9.85(s, 0.53H).



The ^{13}C NMR spectra were scanned >256 times with a repetition time of 30 s; the T_1 of the HCO_3^- was 3 s at 25 °C and shorter at lower temperatures. The overlapped ^1H NMR peaks due to the HSO_3^- isomer and the coalesced hydroxyl protons were decomposed by a double Lorentzian function to obtain peak integrals of each component. Due to the high viscosity of the IL and the resultant line broadening, we could not obtain useful information from ^{17}O NMR.⁴⁷

Raman measurements

Raman spectra were measured at the back scattering geometry by using a doubled output of a Nd:YAG laser (Spectra Physics, Excelsior-532-300) as a probing beam. The scattering light was detected by a Peltier-cooled CCD camera attached to the spectrometer (Princeton Instruments, Insight 256E). The Raman shift was calibrated by the Raman spectra of cyclohexane and benzene in the finger print region, and by the line spectra of a neon lamp at the CH-stretching region. Generally, the sample was enclosed in the NMR tube and the Raman scattering was measured at the room temperature. For the measurement at the low temperature, the temperature was regulated by circulating the temperature controlled water and methanol mixture through the cell holder. The sample was yellowish at $q_{\text{SO}_2} > 1$ and turned green at the laser spot while the Raman spectra were collected. The background signals in the Raman measurement were slightly dependent on the SO_2 loading, which were subtracted by making proper baseline signals by connecting the signal points where no Raman signal detected.

Electronic state calculations

DFT calculations were performed using the basis set of 6-311G+(d,p) or aug-cc-pVTZ and the B3PW91 functional by gaussian-09.⁴⁸

Results and discussion

NMR spectroscopic analysis

We prepared an IL containing sulfur(iv) species by loading various amounts of SO_2 into a dried bicarbonate IL, $[\text{P}_{4448}]\text{HCO}_3^-$. Since SO_2 is a stronger acid than CO_2 , we expect the anion exchange reaction in eqn (1) to occur. In fact, when the bicarbonate IL was brought in contact with SO_2 , evolution of bubbles was observed. To confirm the progress of eqn (1), ^{13}C NMR spectra were collected for each sample. The spectra are shown in Fig. S2.† The bicarbonate anion was observed at 159 ppm in pure $[\text{P}_{4448}]\text{HCO}_3^-$. The peak integral monotonously decreased as the SO_2 injection was repeated, indicating the escape of the bicarbonate anion as gaseous CO_2 . Molecular CO_2 in the IL (which would appear at 125 ppm, if present) was not detected. The cation peak significantly sharpened with the SO_2 uptake which is related to the decrease in viscosity.

^1H NMR spectra for the samples are shown in Fig. 1. In ^1H NMR spectra, a peak emerged at 10 ppm. This peak has not been reported by NMR studies on aqueous bisulfite salts. The chemical shift was insensitive to temperature (Fig. S3†), which indicates that the peak is not of a hydroxyl proton. As

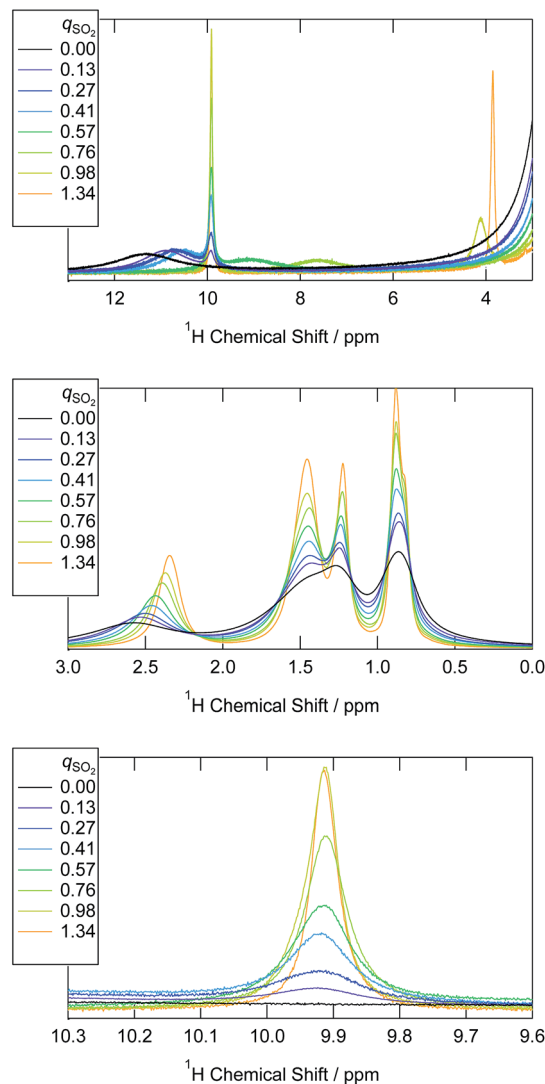


Fig. 1 ^1H NMR spectra of the $[\text{P}_{4448}]\text{HCO}_3^-$ and the ILs that have absorbed SO_2 by various mole ratios (q_{SO_2}) at 298 K.

mentioned in the Introduction, two isomers are proposed for the bisulfite anion (eqn (3)). We elucidate that the peak is due to HSO_3^- , the isomer without the hydroxyl proton. A broad peak was observed spanning from 13 to 10 ppm in $[\text{P}_{4448}]\text{HCO}_3^-$ ($q_{\text{SO}_2} = 0$) and it moved towards 4 ppm as SO_2 loading increased. The peak shifted rightwards at an elevated temperature (Fig. S3†), which indicates hydrogen bonding. Thus we attribute this peak to the species that have hydroxyl protons, namely HCO_3^- and HOSO_2^- . It is presumable that they exchange their protons rapidly and give a single but broad coalesced NMR signal. The drastic chemical shift change with increasing SO_2 loading is ascribed to the decrease of HCO_3^- and the concomitant increase of HOSO_2^- ; the chemical shift of a coalesced peak is the weighted average of the intrinsic chemical shifts of individual components. As established from Fig. 1, these are 12 and 4 ppm for HCO_3^- and HOSO_2^- , respectively. The large chemical shift value of HCO_3^- implies the presence of tight hydrogen bonds, such as those found in the carboxylic acid dimer. The



chemical shift value of HOSO_2^- is typical for a hydrogen-bonded OH group.

The fact that we observe separate ^1H NMR peaks for the two bisulfite isomers HSO_3^- and HOSO_2^- implies that the proton exchanges between the two isomers are relatively slow (>1 s). Such a situation is very different from that in water; in aqueous bisulfite solution, no ^1H NMR peaks other than water is observed. This implies that the two bisulfite isomers rapidly exchange the protons and it is probably mediated by water.

The chemical shift of the α proton (proton attached to the carbon bonded to the P atom) decreased, indicating stronger cation–bicarbonate interactions replaced by weaker cation–bisulfite interactions.

Based on the above peak assignments, we integrated each of the ^1H and ^{13}C NMR peaks and compared the peak integrals with those of the $[\text{P}_{4448}]$ cation. Whenever overlapped peaks were observed, they were decomposed by Lorentzian functions. This allowed us to evaluate the concentration of chemical species i in terms of the mole ratio (q_i) relative to the $[\text{P}_{4448}]$ cation (Fig. 2). The HCO_3^- was quantified by the ^{13}C NMR peak integral (159 ppm). As can be seen from Fig. 2, eqn (1) proceeded quantitatively until the q_{SO_2} reached 1. The HSO_3^- isomer was quantified by the ^1H NMR peak integral (10 ppm). The other isomer was quantified by the coalesced peak for the hydroxyl proton (chemical shift varies) after the HCO_3^- contribution was subtracted. One needs to consider the possibility of the two bisulfite ions condensing to form $\text{S}_2\text{O}_5^{2-}$ as in eqn (2). When this would be the case, 1 equiv. of water may also contribute to the coalesced hydroxyl proton peak. As we will see later, $\text{S}_2\text{O}_5^{2-}$ was not present in samples when $q_{\text{SO}_2} < 1$ according to Raman spectroscopy. Thus, we could safely quantify the HOSO_2^- isomer from the ^1H NMR spectra for $q_{\text{SO}_2} < 1$ as in Fig. 2.

When q_{SO_2} exceeded 1, $q_{\text{HSO}_3^-}$ started to decrease, indicating that HSO_3^- is consumed to form new sulfur(IV) species. These species were not detected by ^1H NMR. In view of high sulfur concentrations, the formation of disulfite ion is plausible. Key

information on the sulfur speciation at $q_{\text{SO}_2} > 1$ is provided by Raman spectroscopy in the next section.

As can be seen from Fig. 2, HSO_3^- is the more abundant of the two bisulfite isomers. The equilibrium quotient of the two isomers ($Q = [\text{HOSO}_2^-]/[\text{HSO}_3^-]$) was in the range of 0.5 ± 0.1 for the 5 samples whose q_{SO_2} was less than 0.8. Knowing that the corresponding equilibrium quotient is reported to be 3–4 for water,^{34,41} the isomer population is reversed in the two solvents.

We consider several plausible reasons for the difference. The first is the absence of hydrogen-bonding in ILs. In an aqueous solution, water molecules form hydrogen bonds more strongly with the isomer that has a hydroxyl group than with one that does not. Thus, the former is more favoured in water than the latter.

The second critical difference is the existence of the Coulomb interactions with cations in ILs. The difference in interactions between bisulfite and phosphonium cation may result in different stabilities of the isomer in ILs. In order to test how the interaction with the cation affects the energetic stability of the isomer, we carried out DFT calculations for HSO_3^- and HOSO_2^- in vapour, in SCRF water, and as a cluster with one $[\text{P}_{4448}]^+$ cation. DFT calculations were done using the basis set aug-cc-pVTZ and B3PW91 functional for the isolated anion in vapour and in SCRF water. For the cluster calculations, we used the 6-311G+(d,p) basis set owing to limitations in computational resources. The optimized structures of the anions and the clusters are shown in Fig. S4 and S5.† Although the cation has conformational flexibility, we limited the calculations for all *trans* and all *gauche* conformations (Fig. S5(a) and (b)†). The energies for the optimized structures are listed in Tables S1 and S2,† and the geometrical parameters are listed in Table S3.† According to the calculations, the HOSO_2^- isomer was stable compared to the HSO_3^- isomer by 10 kJ mol^{-1} in vapour when the aug-cc-pVTZ basis set was used. A similar energy value was calculated for that in SCRF water (10 kJ mol^{-1}) as the model does not include the hydrogen-bonding effect. When we used the 6-311G+(d,p) basis set, the energy difference became somewhat larger (32 kJ mol^{-1}). According to the theoretical estimations of the energy difference between HOSO_2^- and HSO_3^- performed by several groups using MP2 or DFT calculations, the energy difference between these isomers is quite subtle even for the isolated state in vapour, and depends on the basis sets.^{42,43} Our calculation results are consistent with previous estimations⁴² using similar basis sets. The determination of the absolute value at the present level calculation remains challenging. By making clusters with cations, the energy difference between the isomers became somewhat large (41 kJ mol^{-1} for all *trans*, 46 kJ mol^{-1} for all *gauche*). Therefore, by pairing with a cation, the HOSO_2^- isomer is energetically more stable than the HSO_3^- isomer, in contradiction to the expectation from the experimental result. One point to be considered is that the dihedral angles of HO_1SO_2 and HO_1SO_3 of HOSO_2^- (Fig. S4 and S5†) dramatically changed through the complexation with a cation. On the other hand, no significant structure change was calculated for HSO_3^- . This kind of

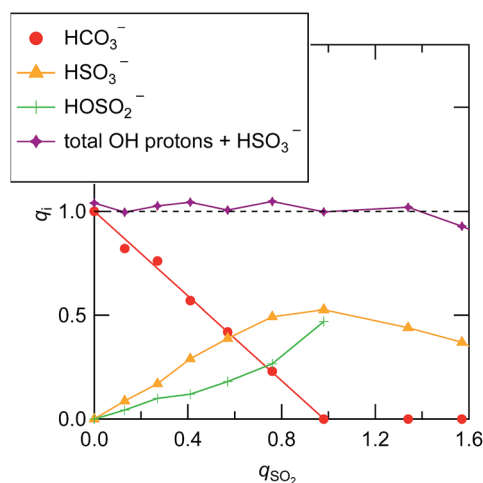


Fig. 2 The abundance of bisulfite isomers and the bicarbonate ion in the ILs with the progress of SO_2 absorption. The vertical axis denotes to the mole ratio with respect to the $[\text{P}_{4448}]$ cation.



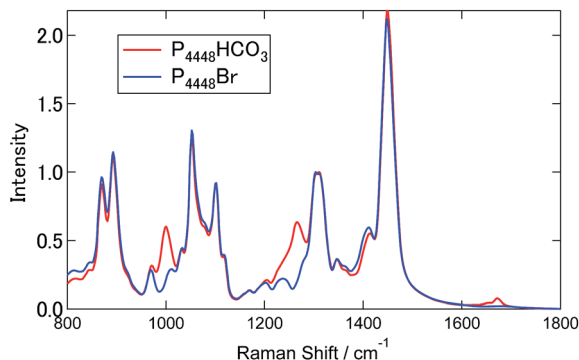


Fig. 3 Raman spectra of $[P_{4448}]Br$ and $[P_{4448}]HCO_3$, respectively.

difference may contribute to isomer stability if more cation molecules surround the anion.

Anion speciation based on Raman spectra

Fig. 3 shows the Raman spectra for $[P_{4448}]Br$ and $[P_{4448}]HCO_3$ in the finger print region. Table S4† summarizes the Raman shifts of the bands observed for these ILs together with those following SO_2 loading on $[P_{4448}]HCO_3$. The following Raman bands in Fig. 3 appeared only for the $[P_{4448}]HCO_3$ sample: 996, 1267, 1655, and 1672 cm^{-1} . In reference to the assignments in aqueous solution,⁴⁹ these bands are $\nu C-OH$, $\nu_s CO_2$, and $\nu_{as} CO_2$ vibrational modes of HCO_3^- . The other bands are assigned to the vibrational modes of $[P_{4448}]^+$, and they do not seem to be affected by the anion exchange from Br^- to HCO_3^- . In the ESI,† DFT calculations are presented for the $[P_{4448}]^+$ vibrational Raman spectra in all *trans* or all *gauche* alkyl-chain conformations using the 6-311G+(d,p) basis set and B3PW91 functional (Fig. S6†). The calculated Raman bands are presented to give the half width at half height of 4 cm^{-1} . The calculation captured majority of the features found in the experimental Raman spectrum. When we used the scaling factor of 0.976 for the horizontal scale, the coincidence between the theory and experiment became much better. The bands could be assigned as follows: (1) the band around 670 cm^{-1} is due to the symmetric stretching mode of the centre P with four connected carbon atoms; (2) the bands around 900 cm^{-1} are mostly in-plane-bending of C-C-H at the terminal CH_3 ; (3) the bands around 1100 cm^{-1} are the bending motions of alkyl-chains; (4) the bands around 1300 cm^{-1} are the wagging motions of C-C-H₂ in the methylene carbons of the alkyl-chain; (5) and the bands around 1450 cm^{-1} are the scissoring motion of HCH.

Fig. 4 shows the Raman spectra of $[P_{4448}]HCO_3$ following SO_2 absorption. The inset figures are the magnifications around 1050 cm^{-1} . Each spectrum is normalized by the band at 1449 cm^{-1} (one of the $[P_{4448}]^+$ vibrations). As the amount of SO_2 increased, several new bands appeared while the HCO_3^- bands (621 cm^{-1} , 996 and 1267 cm^{-1}) diminished. Fig. 5 shows difference spectra from the pure $[P_{4448}]HCO_3$. From $q_{SO_2} = 0$ to 0.98, several new bands (315, 505, and 725 cm^{-1} in Fig. 5(a); 1029, 1048, 1079, and 1120 cm^{-1} in Fig. 5(b)) appeared and their intensities increased with increasing q_{SO_2} . On the other hand,

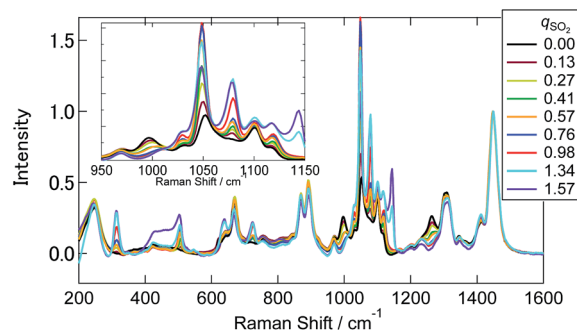


Fig. 4 Raman spectra of $[P_{4448}]HCO_3$ with different q_{SO_2} . The inset figure is the magnification around 1050 cm^{-1} . Each spectrum is normalized by the band at 1449 cm^{-1} .

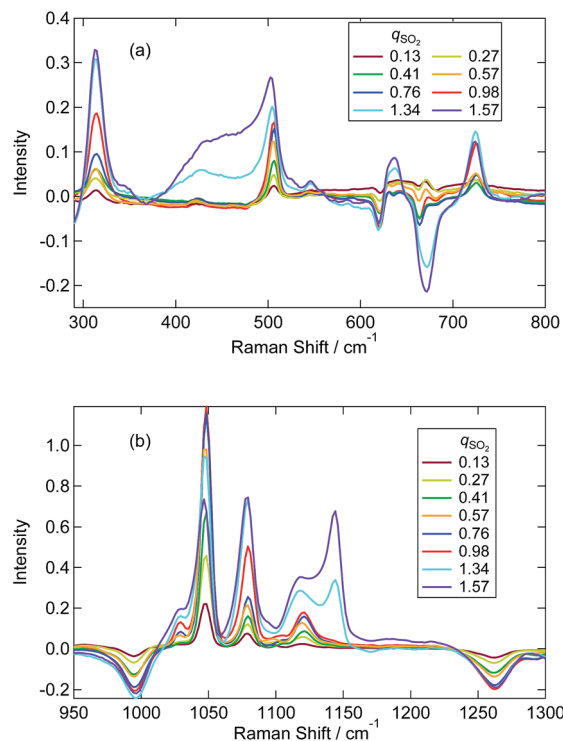


Fig. 5 Difference Raman spectra of $[P_{4448}]HCO_3$ with different q_{SO_2} from neat $[P_{4448}]HCO_3$. (a) From 300 to 800 cm^{-1} . (b) From 950 to 1300 cm^{-1} .

the HCO_3^- bands were shown as dips, which gradually deepened with q_{SO_2} . Further increase of q_{SO_2} from 0.98 to 1.57 resulted in the emergence of a broad band in the 430–500 cm^{-1} range in addition to narrower bands at 635 and 1144 cm^{-1} . A large negative dip appeared around 670 cm^{-1} , suggesting a structural change in the cation.

Raman spectra at the SH and CH stretching vibrations are shown in Fig. 6. The spectrum was normalized by the CH stretching region band center of the $[P_{4448}]^+$ cation (2918 cm^{-1}). A characteristic SH stretching band was found at 2440 cm^{-1} . This assignment is confirmed by the Raman shift in aqueous media (~ 2530 cm^{-1})^{34,36,38,39} and DFT calculations (see below). The intensity of this band increased with increasing q_{SO_2} from



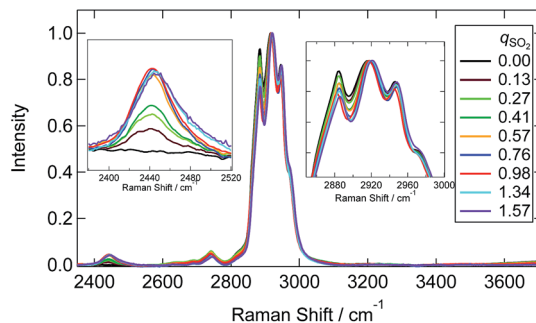


Fig. 6 Raman spectra of $[P_{4448}]HCO_3^-$ with different q_{SO_2} for the SH and CH stretching region. The inset figures are the magnifications around 2450 cm^{-1} and 2920 cm^{-1} respectively. Each spectrum is normalized by the band at 2918 cm^{-1} .

0 to 0.98 and then showed a slight decrease for $q_{SO_2} > 1$. The frequency of this band showed an increase with increasing q_{SO_2} . Interestingly, the lower frequency side band shape of the CH stretching band ($2800\text{--}3000\text{ cm}^{-1}$) changed as the q_{SO_2} increased from 0 to 0.98 and then became almost invariant at higher SO_2 loadings. A slight change of the intensity at the higher frequency side was also noted.

We attempted to assign the characteristic Raman bands particularly seen below 1300 cm^{-1} by tracking the band intensity changes with SO_2 absorption. Based on previous works in aqueous solutions, the following species are plausible: the two bisulfite isomers (HSO_3^- , $HOSO_2^-$), disulfite (pyrosulfite) ion ($S_2O_5^{2-}$), and molecular SO_2 . In water, the disulfite anion is formed by the dehydration of 2 bisulfite anions (eqn (2)). We started by assigning those bands that appear only at $q_{SO_2} > 1$; these are the broad bands around $430\text{--}470\text{ cm}^{-1}$ and two narrower bands at 635 and 1140 cm^{-1} . The band at 1140 cm^{-1} was assigned to SO_2 (physisorption) according to ref. 24 and 26. The bands at 430 and 635 cm^{-1} could be assigned to the vibrations of $S_2O_5^{2-}$ according to ref. 25, which determined corresponding strong bands at 424 and 655 cm^{-1} in water. Later in Sec. 3.3, we will discuss the possibility of $HS_2O_5^-$ instead of $S_2O_5^{2-}$ for $q_{SO_2} > 1$ in more detail. In any case, due to the absence of the marker bands at 1140 cm^{-1} of SO_2 and at 430 cm^{-1} of disulfite for $q_{SO_2} < 1$, we concluded that molecular SO_2 and disulfite were absent for $q_{SO_2} < 1$.

From the above discussion, the plausible origins of the new Raman bands observed at $q_{SO_2} < 1$ are the bisulfite isomers (HSO_3^- , $HOSO_2^-$). The appearance of the SH stretching vibration clearly indicates that the HSO_3^- isomer is present, while we could not detect a clear Raman band for the HO vibration of the other isomer. The HO vibration has been observed by one IR study of aqueous sulfite solutions at 3620 cm^{-1} ,³⁷ and one Raman spectroscopic study at 3145 cm^{-1} .³⁴ The band could be weak, broad or overlapped with C–H vibrations in the IL. The bands at 505 and 1120 cm^{-1} correspond to the aqueous bands observed at $496\text{--}508\text{ cm}^{-1}$ and $1126\text{--}1128\text{ cm}^{-1}$,^{34,36,38} both of which have been assigned to the HSO_3^- in ref. 34. Similarly, we assign the bands at 1079 and 725 cm^{-1} to $HOSO_2^-$ using ref. 34 and 36, respectively, although other reports have not mentioned these bands. The bands near 315 cm^{-1} and 1079 cm^{-1} are

assigned to the vibrations of $S_2O_5^{2-}$ in some publications.^{33,36,39} As discussed in the previous paragraph, however, we have eliminated the presence of $S_2O_5^{2-}$ at $q_{SO_2} < 1$.

We evaluated intensities of Raman bands that appear at different SO_2 loadings by making a multi-peak fit to the difference spectra (Fig. 5(a) and (b)). The detail of the fitting procedure is described in the ESI† and typical examples are shown in Fig. S7(a).† Note that the 996 cm^{-1} dip of HCO_3^- was taken into account by assuming a negative component. Fig. 7 shows the variation of the band intensities as a function of q_{SO_2} . The vibrational frequencies of decomposed bands were almost independent of q_{SO_2} , and the variations were within $\sim 1\text{ cm}^{-1}$ except for the band assigned to the SH vibration (Fig. S7(b)†). To track the band intensity change, the intensities were normalized to unity at equimolar SO_2 loading ($q_{SO_2} = 0.98$). HCO_3^- was quantified using the negative integral area of the HCO_3^- band (996 cm^{-1}) in the difference spectra. When this negative area is normalized, it is the portion (x) of HCO_3^- consumed upon SO_2 absorption. Thus the value was converted to the portion of HCO_3^- that is remaining by $1 - x$. The concentrations of the two bisulfite isomers and HCO_3^- as estimated by NMR in Sec. 3.1 are also shown after the normalization.

As shown in the Fig. 7 the fraction of HCO_3^- as estimated by NMR and Raman agreed quite well. The sulfur-related Raman bands shown in Fig. 7 are divided into two groups based on their q_{SO_2} dependences. The first group includes bands at 505 , 1048 , 1120 , and 2440 cm^{-1} , while the second group includes bands at 315 , 725 , 1029 , and 1079 cm^{-1} . We elucidated that each group of bands arises from one of the two bisulfite isomers. On the basis of NMR spectroscopic abundances, we assigned the first group to the HSO_3^- isomer and the second to the $HOSO_2^-$ isomer. The assignments of the two bisulfite Raman bands at 1029 and 1048 cm^{-1} in aqueous solutions have been ambiguous for decades. In this work, we identified the band at 1048 cm^{-1} as the HSO_3^- vibration and the band at 1029 cm^{-1} as the $HOSO_2^-$ vibration in the IL. The assignment is

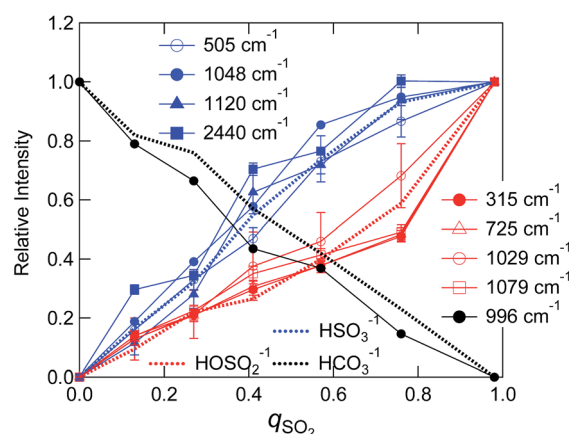


Fig. 7 Dependence of the relative intensity of Raman band on q_{SO_2} . The black broken line represents the relative concentration of HCO_3^- to that at $q_{SO_2} = 0$, and blue and red ones represent the relative concentrations of HSO_3^- and the species having hydroxyl group determined by NMR measurement, respectively.



further confirmed by the fact that the intensity of the 1048 cm^{-1} band corresponded to the NMR measurement above $q_{\text{SO}_2} = 1$ (slight decrease with increasing q_{SO_2}) (not shown in Fig. 7).

The comparison between the experimental difference spectra and the DFT calculations is shown in Fig. 8, and the assignments of bands by the DFT calculations are listed in Table S5.† Although the coincidence between theory and experiment is not so good, it gives us some hints for band assignments. By comparing the calculations, the band at 505 cm^{-1} observed experimentally is the bending mode of SO_2 in HSO_3^- , the band at 1048 cm^{-1} is the symmetric stretching mode of SO_2 in HSO_3^- , and the band at 1120 cm^{-1} is the bending mode of OSH . As for the HOSO_2^- vibrations, the band at 315 cm^{-1} is the bending mode of OS(OH) , and the bands at 1029 and 1079 cm^{-1} are the combinations of the bending band of SOH with SO stretching vibration and SO_2 symmetric stretching vibration, respectively.

A few remarks must be made regarding band assignments. First, the intensity of the band at 1120 cm^{-1} assigned to the HSO_3^- vibration remarkably increased above $q_{\text{SO}_2} = 1$, although the concentration of HSO_3^- decreased according to the NMR result. This may be due to the overlapping with sulfur species that forms above $q_{\text{SO}_2} = 1$. Second, the ν_{SH} band at 2440 cm^{-1} in the IL shows a significant lower frequency shift relative to the corresponding band in the aqueous solution (2530 cm^{-1}).^{34,36,38,39} The S–H bonding may be weakened in the IL due to the interaction with the surrounding cations. The SH frequency shows an increase with increasing q_{SO_2} (Fig. S7(b)†). This suggests that not only is the interaction with the cation important for SH frequency, but so is the one with the anion.

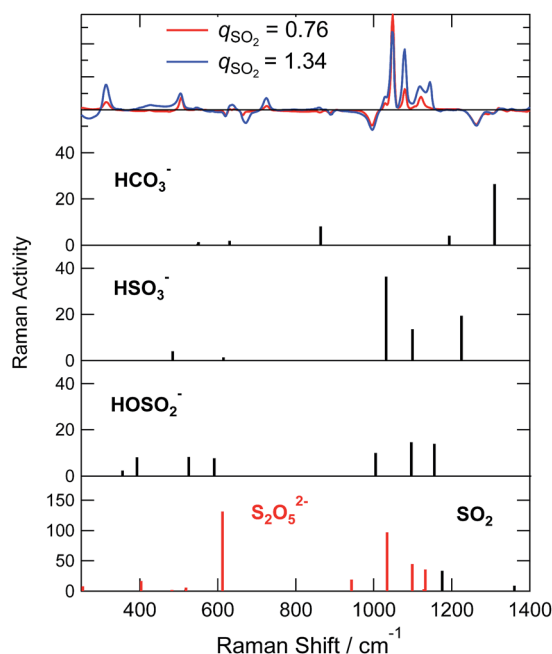


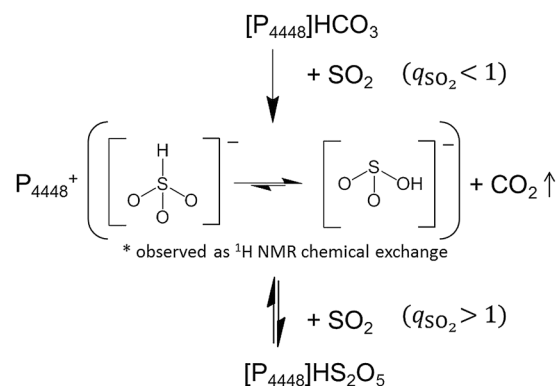
Fig. 8 Vibrational spectra of different anions calculated by DFT using aug-cc-pVTZ basis set and B3PW91 functional. The upper panel shows difference Raman spectra of $[\text{P}_{4448}]\text{HCO}_3$ with different q_{SO_2} from neat $[\text{P}_{4448}]\text{HCO}_3$.

Third, our DFT calculations did not reproduce the band at 725 cm^{-1} . As previously reported, a difficulty exists in the calculation for the S–O(H) mode⁴³ and a theoretical model inadequacy may be the reason. As for another plausible reason for the lack of band reproduction, at first we considered that the complexation with cation may produce a shift of the band. As shown in the calculated spectra in Fig. S8,† the computational Raman spectra of HCO_3^- and HOSO_2^- with a cation showed a relatively large shift probably due to the nature of asymmetric complex formation. However, we could not identify a band at 725 cm^{-1} for these complexes. Zhang and Ewing proposed the existence of the HOSO_2^- dimer.³⁷ Although we performed the calculation for this species in vapour, it was not stable. The calculation in water (SCRF model) converged and two stable isomers of the HOSO_2^- dimer were calculated. The optimized structures are shown in Fig. S9(a) (symmetric dimer) and (b) (asymmetric dimer).† The geometrical parameters are listed in Table S6.† Calculated Raman spectra are shown in Fig. S9(c).† The vibrational band around 700 cm^{-1} was calculated by making a dimer in either symmetric or asymmetric conformation. This band is due to the vibration of S(OH) symmetric stretching in both sides. The calculations suggest the possibility of HOSO_2^- dimer formation. The quadratic dependence of HCO_3^- and HOSO_2^- concentrations on q_{SO_2} in Fig. 7 may be due to the HOSO_2^- dimer formation.

SO₂ absorption mechanism

Based on the spectroscopic observations, the SO_2 absorption by $[\text{P}_{4448}]\text{HCO}_3$ consists of two phases; see Scheme 1. In the first phase (below $q_{\text{SO}_2} = 1$), the bicarbonate anion is quantitatively replaced by SO_2 as in eqn (1) until the mole of absorbed SO_2 reaches the initial mole of bicarbonate ($q_{\text{SO}_2} = 1$). The absorbed SO_2 is present either as HSO_3^- or HOSO_2^- (eqn (3)), which are in equilibrium. Condensation of bisulfite to form disulfite (eqn (2)) is negligible within the first phase. At $q_{\text{SO}_2} = 1$, the ionic liquid turns into pure $[\text{P}_{4448}][\text{bisulfite}]$ by complete “gas exchange”. Above $q_{\text{SO}_2} = 1$ (the second phase), SO_2 is absorbed by another mechanism which will be discussed in the followings.

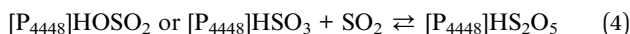
The $[\text{P}_{4448}][\text{bisulfite}]$ liquid can further absorb SO_2 and the q_{SO_2} nearly reaches 1.6 at SO_2 partial pressure less than 0.1 MPa.



Scheme 1 Proposed SO_2 chemisorption mechanism by the bicarbonate ionic liquid $[\text{P}_{4448}]\text{HCO}_3$.



It is argued here what is the actual chemical form of the newly absorbed SO_2 . We postulate the following Lewis acid–base reaction.



We have no information on which of the two bisulfite isomers is more reactive. Molecular SO_2 has Lewis basic character as well as Lewis acidic character.⁵⁰ The adducts of SO_2 with electron-rich species such as amines and halide ions are well known.^{50,51} As is mentioned in the Introduction, bromide in 1-butyl-3-methylimidazolium bromide ionic liquid can capture SO_2 by a charge-transfer interaction.²¹ The charge-transfer interaction is evidenced by a yellowish or orange colour of the solution and the low frequency shift of the $\nu_s(\text{SO}_2)$ Raman band. In our system, both a colour change (colourless at $q_{\text{SO}_2} < 1$ and turned into bright yellow at $q_{\text{SO}_2} > 1$) and a Raman band shift (from 1152 cm^{-1} in water³⁸ to 1144 cm^{-1} in the IL) were observed.

In the $q_{\text{SO}_2} > 1$ absorption phase, three intense Raman bands have emerged (~ 430 , 635 , $\sim 1050 \text{ cm}^{-1}$). These Raman bands nearly coincide with some of the strongest bands of $\text{S}_2\text{O}_5^{2-}$. On the other hand the Raman bands for HS_2O_5^- has not been reported. Given the structural similarity, these two ionic species may not be distinguished only from Raman spectra.

The $\text{S}_2\text{O}_5^{2-}$ can form *via* the condensation of two bisulfite ions as in eqn (2). We have shown that this reaction does not occur below $q_{\text{SO}_2} = 1$. Then, it seems unreasonable to imagine the reaction abruptly switched on above $q_{\text{SO}_2} = 1$. Thus we may assign the observed Raman bands to HS_2O_5^- , which has been formed *via* eqn (4).

In order to test the above idea, we completed DFT calculations for HS_2O_5^- . The calculations showed that both HOSO_2^- and HSO_3^- make stable complexes with SO_2 to form HS_2O_5^- with stabilization energies of 68 kJ mol^{-1} and 60 kJ mol^{-1} , respectively, at the aug-cc-pVTZ and B3PW91 level calculations in vacuum (Table S1†). Fig. S10(a) and (b)† show the structure of the optimized cluster and Table S7† summarizes the geometrical parameters. The Mulliken charge of SO_2 was -0.55 for the complex with HOSO_2^- , and -0.20 for the complex with HSO_3^- . This clearly indicates that the complexation is due to the charge transfer process. The extent of the charge transfer was more significant for the former complex. The vibrational Raman spectra are compared for $\text{S}_2\text{O}_5^{2-}$ and the complex between SO_2 and bisulfite in Fig. S7(e)†. The intense band at 400 cm^{-1} for $\text{S}_2\text{O}_5^{2-}$ is the combination of the wagging motion of the SO_2 side and the bending motions of SO_2 in the SO_3 side, the band at 612 cm^{-1} is the umbrella mode of SO_3 , the band at 1034 cm^{-1} is the symmetric vibration of S_2O_5 , and the band at 1099 cm^{-1} is the asymmetric vibration of S_2O_5 . For the complex of HOSO_2^- or HSO_3^- with SO_2 , similar vibrational modes were calculated as split bands near the frequencies for $\text{S}_2\text{O}_5^{2-}$. Based on these results, chemisorption of eqn (4) is consistent with experimental observations as the SO_2 absorption mechanism for $q_{\text{SO}_2} > 1$.

In summary the absorption scheme of SO_2 by $[\text{P}_{4448}]\text{HCO}_3$ is illustrated in Scheme 1. Below $q_{\text{SO}_2} = 1$, SO_2 is absorbed by the

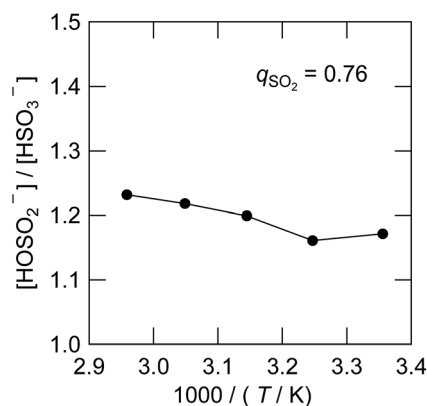


Fig. 9 Temperature dependence of the isomeric equilibrium quotient between HSO_3^- and HOSO_2^- at $q_{\text{SO}_2} = 0.76$.

IL in replacement with CO_2 as HSO_3^- or HOSO_2^- , where they are in equilibrium. Above $q_{\text{SO}_2} = 1$, SO_2 is absorbed by the IL making the charge transfer complexes with HSO_3^- or HOSO_2^- .

Isomerization equilibrium and kinetics

The equilibrium quotient of the bisulfite isomers is reported to be dependent on temperature in water by ^{17}O -NMR⁴¹ and XANES³⁴ studies. The quotient changes by a factor of 2 with the temperature change of 40 K ,⁴¹ with the HOSO_2^- isomer favoured more at lower temperatures. In Fig. 9, we determined the corresponding value in the IL using the ^1H NMR spectra presented in Fig. S3.† As can be seen, the value changed only by 5% with the temperature change of 40 K . The striking difference between water and the IL solvent can be interpreted by the solvation of the HOSO_2^- isomer. Only in water is the HOSO_2^- isomer hydrogen-bonded to the solvent. Since the hydrogen bond is stronger at lower temperature, we expect the HOSO_2^- isomer to be more abundant in low temperature water but such a temperature effect is not expected in the IL. We have also

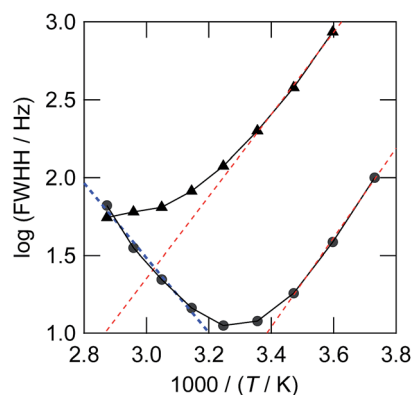


Fig. 10 ^1H NMR full width at half height (FWHH) at $268\text{--}348 \text{ K}$. The FWHH for the HSO_3^- isomer and the coalesced hydroxyl protons (HOSO_2^- and HCO_3^-) are shown by circles and triangles, respectively. The red thin dashed lines show the natural width. The thick blue dashed line shows the line broadening of the HSO_3^- peak due to the isomer exchange of eqn (3).



confirmed that the Raman spectra were not dependent on temperature from 296 K to 253 K for the sample of $q_{\text{SO}_2} = 0.76$.

In order to detect any proton exchanges between the two bisulfite isomers, we plotted the width (full width at half height or FWHH) of the ^1H NMR peaks for the HSO_3^- and hydroxyl protons against temperature in Fig. 10. The FWHH in the low temperature region could be fitted to an exponential function (red dashed lines). In this region, the FWHH is controlled by the solvent viscosity. It is remarkable that the FWHH's of HSO_3^- and hydroxyl protons deviate from the viscosity trend at higher temperatures. This is reasoned by a line broadening due to the chemical exchange, the rate of which exponentially increases with temperature (blue dashed line). The spin dynamics theory states that the FWHH in the Hz unit is proportional to the first order rate constant of the proton exchange reaction k . At 320 K, the value of k is estimated to be $\sim 10 \text{ s}^{-1}$. The blue dashed lines demonstrate that the FWHH follows the Arrhenius-type temperature dependence. From the slope, we determined the activation energy of the bisulfite anion exchange to be $46 \pm 4 \text{ kJ mol}^{-1}$.

Conclusions

Herein, for the first time, we have reported NMR and Raman spectroscopic observations for bisulfite IL, which is prepared via "gas exchange" of bicarbonate ionic liquid. Both Raman and NMR spectra have indicated that the bisulfite anion is subject to isomerization. One of the isomers has an SH bond (HSO_3^-) that is characterized by a signal at 10 ppm by ^1H NMR and the Raman bands at 506, 1048, 1120 and 2440 cm^{-1} . The other isomer has an OH bond (HOSO_2^-) that is characterized by the Raman bands at 314, 725, 1029 and 1079 cm^{-1} . The isomerization equilibrium in the IL is shifted to the HSO_3^- side compared to that in water. The bisulfite IL absorbs excess SO_2 by making the charge transfer complex with bisulfite anions as elucidated by Raman bands at 430–500 (broad), 635, and 1140 cm^{-1} .

Acknowledgements

This work is partially supported by MEXT-Supported Program for the Strategic Research Foundation at Private Universities 2015–2019 (S1511025). We thank Prof. M. Ueno (Doshisha University) for useful discussions.

Notes and references

- Z. Lei, C. Dai and B. Chen, *Chem. Rev.*, 2014, **114**, 1289.
- (a) R. Quinn, J. B. Appleby and G. P. Pez, *J. Am. Chem. Soc.*, 1995, **117**, 329; (b) R. Quinn, *Synth. React. Inorg. Met.-Org. Chem.*, 2001, **31**, 359.
- E. D. Bates, R. D. Mayton, I. Ntai and J. H. J. Davis, *J. Am. Chem. Soc.*, 2002, **124**, 926.
- E. G. Maginn, *Quarterly Technical Report to U. S. DOE, 01/05–03/05*, DOE Scientific and Technical Information, Oak Ridge, TN, 2005, p. 1.
- (a) A. Yokozeki, M. B. Shiflett, C. P. Junk, L. M. Grieco and T. Foo, *J. Phys. Chem. B*, 2008, **112**, 16654; (b) M. B. Shiflett and A. Yokozeki, *J. Chem. Eng. Data*, 2009, **54**, 108; (c) M. B. Shiflett, D. W. Drew, R. A. Cantini and A. Yokozeki, *Energy Fuels*, 2010, **24**, 5781.
- H. Yang, Z. Xu, M. Fan, R. Gupta, R. B. Slimane, A. E. Bland and I. Wright, *J. Environ. Sci.*, 2008, **20**, 14.
- D. Camper, J. E. Bara, D. L. Gin and R. D. Noble, *Ind. Eng. Chem. Res.*, 2008, **47**, 8496.
- G. Puxty, R. Rowland, A. Allport, Q. Yang, M. Bown, R. Burns, M. Maeder and M. Attalla, *Environ. Sci. Technol.*, 2009, **43**, 6427.
- Y. Zhang, S. Zhang, X. Lu, Q. Zhou, W. Fan and X. Zhang, *Chem.-Eur. J.*, 2009, **15**, 3003.
- B. E. Gurkan, J. Fuente, E. M. Mindrup, L. E. Ficke, B. F. Goodrich, E. A. Price, W. F. Schneider and J. F. Brennecke, *J. Am. Chem. Soc.*, 2010, **132**, 2116.
- L. Sanchez, G. Meindersma and A. De Haan, *Chem. Eng. J.*, 2010, **166**, 11.
- C. Wang, H. Luo, D. Jiang, H. Li and S. Dai, *Angew. Chem., Int. Ed.*, 2010, **49**, 5978.
- G. Gurau, H. Rodriguez, S. P. Kelley, P. Janiczek, R. Kalb and R. D. Rogers, *Angew. Chem., Int. Ed.*, 2011, **50**, 12024.
- (a) G. Wang, W. Hou, F. Xiao, J. Geng, Y. Wu and Z. Zhang, *J. Chem. Eng. Data*, 2011, **56**, 1125; (b) G. N. Wang, Y. Dai, X. B. Hu, F. Xiao, Y. T. Wu, Z. B. Zhang and Z. Zhou, *J. Mol. Liq.*, 2012, **168**, 17.
- M. I. Cabaço, M. Besnard, Y. Danten and J. A. P. Coutinho, *J. Phys. Chem. A*, 2012, **116**, 1605.
- (a) S. Stevanovic, A. Podgoršek, A. A. H. Padua and M. F. C. Gomes, *J. Phys. Chem. B*, 2012, **116**, 14416; (b) S. Stevanovic, A. Podgoršek, L. Moura, C. C. Santini, A. A. H. Padua and M. F. Costa Gomes, *Int. J. Greenhouse Gas Control*, 2013, **17**, 78.
- (a) S. Kasahara, E. Kamio, T. Ishigumi and H. Matsuyama, *Chem. Commun.*, 2012, **48**, 6903; (b) S. Kasahara, E. Kamio and H. Matsuyama, *J. Membr. Sci.*, 2014, **454**, 155.
- (a) Y. Yasaka, M. Ueno and Y. Kimura, *Chem. Lett.*, 2014, **43**, 626; (b) Y. Yasaka and Y. Kimura, *J. Chem. Eng. Data*, 2016, **61**, 837.
- W. Shi, R. I. Thompson, E. Albenze, J. A. Steckel, H. B. Nulwala and D. R. Luebke, *J. Phys. Chem. B*, 2014, **118**, 7383.
- J. L. Anderson, J. K. Dixon, E. J. Maginn and J. F. Brennecke, *J. Phys. Chem. B*, 2006, **110**, 15059.
- R. A. Ando, L. J. A. Siqueira, F. C. Bazito, R. M. Torresi and P. S. Santos, *J. Phys. Chem. B*, 2007, **111**, 8717.
- D. Yang, M. Hou, H. Ning, J. Ma, X. Kang, J. Zhang and B. Han, *ChemSusChem*, 2013, **6**, 1191.
- S. Zeng, H. He, H. Gao, X. Zhang, J. Wang, Y. Huang and S. Zhang, *RSC Adv.*, 2015, **5**, 2470.
- Y. Shang, H. Li, S. Zhang, H. Xu, Z. Wang, L. Zhang and J. Zhang, *Chem. Eng. J.*, 2011, **175**, 324.
- W. Wu, B. Han, H. Gao, Z. Liu, T. Jiang and J. Huang, *J. Phys. Chem.*, 2004, **43**, 2415.
- M. B. Shiflett and A. Yokozeki, *Ind. Eng. Chem. Res.*, 2010, **49**, 1370.



- 27 S. Ren, Y. Hou, W. Wn, Q. Liu, Y. Xiao and X. Chen, *J. Phys. Chem. B*, 2010, **114**, 2175.
- 28 K. Huang, G.-N. Wang, Y. Dai, Y.-T. Wu, X.-B. Hu and Z.-B. Zhang, *RSC Adv.*, 2013, **3**, 16264.
- 29 G. Cui, F. Zhang, X. Zhou, Y. Huang, X. Xuan and J. Wang, *ACS Sustainable Chem. Eng.*, 2015, **3**, 2264.
- 30 V. A. Simon and K. Waldemann, *Z. Anorg. Allg. Chem.*, 1956, **284**, 36.
- 31 A. Simon and H. Kriegesmann, *Chem. Ber.*, 1956, **89**, 2442.
- 32 V. A. Simon and K. Waldemann, *Z. Anorg. Allg. Chem.*, 1956, **283**, 359.
- 33 B. Meyer, L. Peter and C. Shaskey-Rosenlund, *Spectrochim. Acta, Part A*, 1979, **35**, 345.
- 34 E. D. Risberg, L. Eriksson, J. Mink, L. G. M. Pettersson, M. Y. Skripkin and M. Sandström, *Inorg. Chem.*, 2007, **46**, 8332.
- 35 A. W. Herlinger and T. V. Long II, *Inorg. Chem.*, 1969, **8**, 2661.
- 36 R. E. Connick, T. M. Tam and E. von Deuster, *Inorg. Chem.*, 1982, **21**, 103.
- 37 Z. Zhang and G. E. Ewing, *Spectrochim. Acta, Part A*, 2002, **58**, 2105.
- 38 B. Meyer, M. Ospina and L. B. Peter, *Anal. Chim. Acta*, 1980, **117**, 301.
- 39 D. Littlejohn, S. A. Walton and S.-G. Chang, *Appl. Spectrosc.*, 1992, **46**, 848.
- 40 I. Lindqvist and M. Mörtzell, *Acta Crystallographica*, 1957, **10**, 406.
- 41 D. A. Horner and R. E. Connick, *Inorg. Chem.*, 1986, **25**, 2414.
- 42 R. E. Brown and F. Barber, *J. Phys. Chem.*, 1995, **99**, 8071.
- 43 M. A. Vincent, I. J. Palmer and I. H. Hillier, *J. Mol. Struct.: THEOCHEM*, 1997, **394**, 1.
- 44 J. A. Noblet and K. A. Schugart, *J. Mol. Struct.: THEOCHEM*, 1994, **341**, 1.
- 45 R. M. Golding, *J. Chem. Soc.*, 1960, 3711.
- 46 D. A. Horner and R. E. Connick, *Inorg. Chem.*, 2003, **42**, 1884.
- 47 Horner and Connick reported in ref. 14 that the ^{17}O NMR signals for the two isomers are separated by 20 ppm. The spectral width of the peaks in the IL has turned out to be ~ 100 ppm at 298 K.
- 48 M. J. Frisch, *et al.*, *Gaussian 09, Revision D.01*.
- 49 W. W. Rudolph, G. Irmer and E. Königsberger, *Dalton Trans.*, 2008, 900–908.
- 50 F. A. Cotton, G. Wilkinson, and P. L. Gaus, *Basic Inorganic Chemistry*, Wiley, New York, NY, 3rd edn, sec. 19–5, 1995.
- 51 W. Eisfeld and M. Regitz, *J. Am. Chem. Soc.*, 1996, **118**, 11918.

